On Eastern Asian Dust Storm

Zhao Bolin (赵柏林) and *Yu Xiaoding* (俞小鼎)
Department of Geophysics, Peking University, Beijing 100871
Received November 10, 1988

ABSTRACT

In this paper, the characteristics of eastern Asian dust storm are examined with emphasis on the satellite measurements of aerosol optical thickness. The reflectivity of solar radiation from the earth's atmosphere depends on the optical thickness. The satellite measurement of radiance of sunlight, scattered by the earth and its atmosphere, is used to derive the properties of aerosol on oceanic surfaces. This paper involves the following: (1) investigation of the measurement of dust storm over the oceanic surface by GMS satellite; (2) investigation of the measurement of dust storm over the land surface by ground–based instruments such as actinometer, lidar, etc.; (3) for comparison, deriving an atmospheric aerosol size distribution over the oceanic surface of calm weather through measurements of NOAA satellite; and (4) the weather process and its mass load of eastern Asian dust storm.

1. INTRODUCTION

Recently people are concerned about air pollution which has been becoming increasingly serious year by year. The concentration of atmospheric aerosol is increasing rapidly, while the transparency of the atmosphere is decreasing obviously, affecting thus global climate and human life. The dust storm is an important source of atmospheric aerosol. The Saharan dust haze, which accounts for about 25% of the global water–insoluble aerosol content, is an essential climatological feature. The eastern Asian dust storm (EADS) is another important source of atmospheric aerosol.

In China about 1000 counties keep historical weather records concerning flood, drought, dust storm, etc. Based on ancient Chinese records of dust rain, the map of places and moving path of dust fall have been drawn in Figs. 1 and 2 (Zhang, 1984). EADS is usually associated with strong cyclone, shifts from north to south accompanying with strong wind, and sometimes even sweeps almost all over the country. According to the calculation it might be obtained that the moving speed of the dust is about 12 degrees of longitude / per day or 11.8 m / s, which approaches the mean westerly component between 700–500 hPa at the same time. The EADS, coming from North–west China and Mid–Asian, passes through China main land, Japan, usually till to Hawaii. From October to next May, there are 8–10 times of dust storm. Most of them are in March and April. The strong dust storm often covers a half of China, and extends to the Pacific Ocean. From the chemical analysis of aerosol of Hawaii, Parrington (1983) found that the maximum concentration of aluminium happens in the months when the EADS occurs frequently, but this effect has not been revealed for sea sodium (Fig. 3). Aluminium is one of the main compositions of the land aerosol.

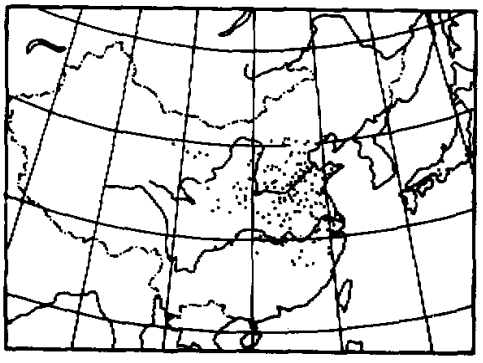

Fig. 1. The places of dust fall in historical times (Zhang, 1984).

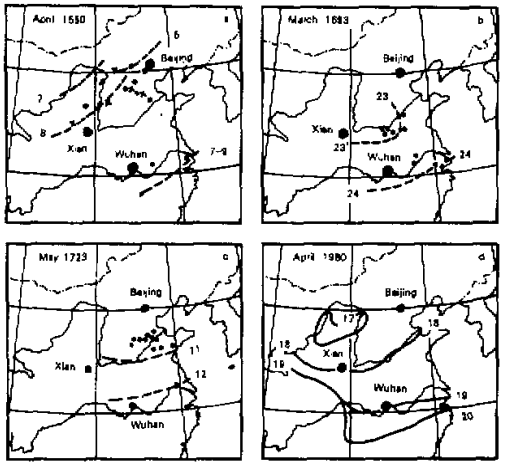

Fig. 2. The sketch maps of moving path of the dust fall (Zhang, 1984).

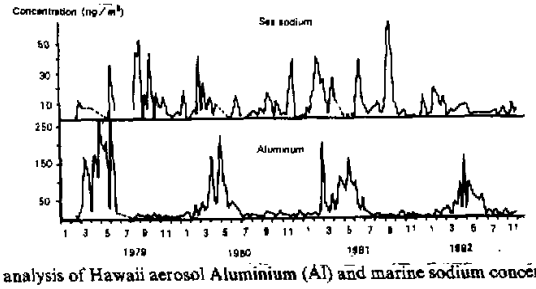

Fig. 3. Chemical analysis of Hawaii aerosol Aluminium (Al) and marine sodium concentration of aerosols collected at MLO Hawaii (Parrington et al., 1983).

II. SATELLITE REMOTE SENSING OF DUST STORM

From the radiative transfer equation, we found that in a dust storm system, the

reflectivity of solar radiation depends on the optical thickness. The larger the optical thickness, the larger the reflectivity will be. The contour of dust storm can be found in satellite pictures.

The satellite measurements of the radiance of sunlight scattered by the earth and its atmosphere, can be used to derive the properties of aerosol. In this paper, the emphasis is put on the satellite measurements of aerosol optical thickness and its mass load on oceans. The main issues are as follows: (1) investigation of the Asian dust storm by the measurements from VISSR radiometer (visible) of GMS; (2) investigation of atmospheric aerosol of clear sky on oceans by the measurements of AVHRR radiometer (visible) on board NOAA–7; and (3) comparison of the results with those obtained by ground–based instruments on land, such as actinometer, lidar, etc.

1. *The radiative transfer equations are solved by approximate method:*

$$-\mu\frac{dI^{-}(\tau,\ \mu,\ \varphi)}{d\tau}=I^{-}(\tau,\ \mu,\ \varphi)-\frac{1}{4\pi}\int_0^1\int_0^{2\pi}p(\mu,\ \mu',\ \varphi,\ \varphi')I^{-}(\tau,\ \mu',\ \varphi')d\mu'd\varphi'$$
$$-\frac{1}{4\pi}\int_0^1\int_0^{2\pi}I^{+}(\tau,\ \mu',\ \varphi')p(\mu,\ -\mu',\ \varphi,\ \varphi')d\mu'd\varphi'-\frac{S_\lambda}{4\pi}e^{-\tau/\mu_0}p(\mu,\ \mu_0,\ \varphi), \tag{1}$$

$$\mu\frac{dI^{+}(\tau,\ \mu,\ \varphi)}{d\tau}=I^{+}(\tau,\ \mu,\ \varphi)-\frac{1}{4\pi}\int_0^1\int_0^{2\pi}p(\mu,\ \mu',\ \varphi,\ \varphi')I^{+}(\tau,\ \mu',\ \varphi')d\mu'd\varphi'$$
$$-\frac{1}{4\pi}\int_0^1\int_0^{2\pi}I^{-}(\tau,\ \mu',\ \varphi')p(\mu,\ -\mu',\ \varphi,\ \varphi')d\mu'd\varphi'-\frac{S_\lambda}{4\pi}e^{-\tau/\mu_0}p(\mu,\ -\mu_0,\ \varphi), \tag{2}$$

where I^{+}, I^{-} upward and downward radiances,

τ optical depth,

μ, μ' $\cos\theta$ and $\cos\theta'$,

θ, θ' zenith angles,

φ, φ' azimuthal angles,

θ_0 solar zenith angle,

$p(\mu,\ \mu',\ \varphi,\ \varphi')$ scattering phase function,

πS_λ incident collimated flux crossing a unit area.

$$\omega_0=\frac{1}{4\pi}\int_{-1}^{+1}\int_0^{2\pi}p(\mu,\ \mu',\ \varphi,\ \varphi')d\mu'd\varphi', \tag{3}$$

is the single scattering albedo.

With Kaufman's (1979, 1982) approximate method, the solutions can be derived as follows:

$$I^{+}(\tau,\ \mu,\ \varphi)=D_1e^{\tau/\mu}+\frac{U_1e^{K\tau}}{1-\mu K}+\frac{U_2e^{-K\tau}}{1+\mu K}+\frac{U_3e^{-\frac{\tau}{\mu_0}}}{1+\frac{\mu}{\mu_0}} \tag{4}$$

where

$$U_1=A\left(\frac{\omega_0}{\pi}\right)\left[1-\beta(\mu)+\frac{\beta(\mu)}{\gamma_2}(\gamma_1-K)\right];$$

$$U_2 = B\left(\frac{\omega_0}{\pi}\right)\left[1-\beta(\mu)+\frac{\beta(\mu)}{\gamma_2}(\gamma_1+K)\right];$$

$$U_3 = C\left(\frac{\omega_0}{\pi}\right)\left[1-\beta(\mu)\right]+\frac{\omega_0}{\pi}\frac{\beta(\mu)}{\gamma_2}\left[C_1\left(\gamma_1+\frac{1}{\mu_0}\right)-\pi S_\lambda\omega_0\beta_0\right]$$
$$+\frac{S_\lambda}{4}p(\mu_1-\mu_0,\ \varphi);$$

$$D_1 = e^{-\tau_0/\mu}\left[\frac{\eta(\theta_0,\ \theta,\ \varphi)F^+(\tau_0)}{\pi}-\frac{U_1e^{K\tau_0}}{1-\mu K}-\frac{U_2e^{-K\tau_0}}{1+\mu K}-\frac{U_3e^{-\tau_0/\mu_0}}{1+\mu/\mu_0}\right];$$

$$K=(\gamma_1^2-\gamma_2^2)^{\frac{1}{2}};$$

and

$$A=\left\{B(\gamma_1+K)+\left[C\left(\gamma_1+\frac{1}{\mu_0}\right)-\pi S_\lambda\omega_0\beta_0\right]\right\}/(K-\gamma_1);$$

$$B=\{E_1e^{K\tau_0}+E_2e^{-\tau_0/\mu_0}\}/\{E_3e^{K\tau_0}+E_4e^{-K\tau_0}\};$$

$$C=\pi S_\lambda\omega_0\left\{\frac{\beta_0}{\mu_0}-\gamma_1\beta_0-\gamma_2(1-\beta_0)\right\}\frac{\mu_0^2}{1-K^2\mu_0^2};$$

$$E_1=\left[C\left(\gamma_1+\frac{1}{\mu_0}\right)-\pi S_\lambda\omega_0\beta_0\right]\left[\frac{1}{\gamma_1-K}-\frac{R}{\gamma_2}\right];$$

$$E_2=-C+\pi S_\lambda\mu_0R+\frac{R}{\gamma_2}\left[C\left(\gamma_1+\frac{1}{\mu_0}\right)-\pi S_\lambda\omega_0\beta_0\right];$$

$$E_3=(\gamma_1+K)\left[-\frac{1}{\gamma_1-K}+\frac{R}{\gamma_2}\right];$$

$$E_4=1-\frac{R}{\gamma_2}(\gamma_1+K);$$

$$F^-(\tau_0)=R[\pi S_\lambda\mu_0e^{-\tau_0/\mu_0}+F^-(\tau_0)];$$

$$F^-(\tau_0)=\frac{1}{\gamma_2}\left\{A(\gamma_1-K)e^{K\tau_0}+\left[C\left(\gamma_1+\frac{1}{\mu_0}\right)-\pi S_\lambda\omega_0\beta_0\right]e^{-\tau_0/\mu_0}\right.$$
$$\left.+B(\gamma_1+K)e^{-K\tau_0}\right\};$$

$$\gamma_1=2[1-\omega_0(1-\beta')];\quad \gamma_2=2\omega_0\beta';\quad \beta'=\int_0^1\beta(\mu)d\mu;$$

$$\beta(\mu)=\frac{1}{4\pi\omega_0}\int_0^1\int_0^{2\pi}p(\mu,\ \mu',\ \varphi,\ \varphi')d\varphi'd\mu';\quad \beta_0=\beta(\mu_0);$$

R is the surface albedo, and $\eta\ (\theta_0,\ \theta,\ \varphi)$ the ratio of reflectivity at $(\theta,\ \varphi)$ to the mean value. Then the relationship between aerosol optical thickness and reflective radiance of sunlight can be obtained.

In the visible band, the columnar dust concentration is directly proportional to optical thickness. Having carried out a set of experiments, Griggs (1979) found that on the surface, the atmospheric optical thickness derived from ground-based volt-photometer measurement

is comparable with that obtained from radiance observation of satellite, because the optical thickness is directly proportional to the radiance from satellite observations. The atmospheric aerosol on oceans can be obtained from the satellite-observed radiance, with error about 10%.

2. *Parameters*

(1) *Spectrum and refractive index (Otterman 1982; Iwasaka 1983)*

Junge's distribution has been used

$$dN / \lg r = Cr^{-v}, \tag{5}$$

where r is the radius, and N the concentration. Iwasaka (1983) suggested $v=2.5$ for dust storm case.

The refractive index m is

$$m = n_r - n_i, \tag{6}$$

where n_r and n_i are the real and imaginary parts of refractive indexes, respectively. For Sahara dust, $n_r=1.525$— 1.56, and $n_i=0$— 0.0055; and for western Asian dust, $n_r=1.5$—1.6, and $n_i=0.001\pm0.001$.

(2) *Phase function*

The phase function of Junge spectrum with $v=2.5$ and 3.0 is depicted in Fig. 4, showing that the difference of these two curves is very small between $\theta=30^\circ-160^\circ$.

(3) *Upward radiance*

Upward radiance of Junge distribution with $v=2.5$ and 3.0 is shown in Fig. 5. The difference between them is smaller than 5%. So that parameter γ is insensitive.

(4) *Atmospheric scattering*

It is much greater than atmospheric absorption in the visible band. Usually,

$$\tau_0 = \tau_R + \tau_a. \tag{7}$$

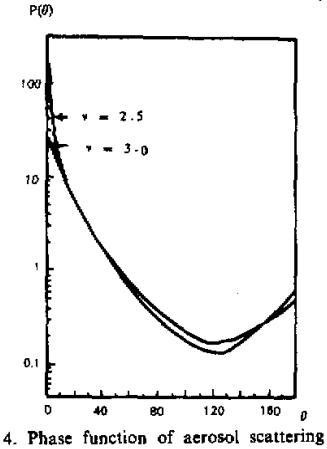

Fig. 4. Phase function of aerosol scattering (Junge formula $n_r=1.50, n_i=0, \lambda=0.65\mu m$).

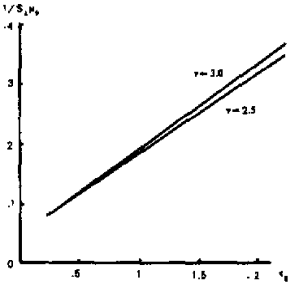

Fig. 5. Reflective radiance depends upon particular spectrum $I/S_\lambda\mu_0$: reflectivity τ_o: atmospheric optical thickness v: parameter of Junge spectrum (Junge spectrum, $n_r=1.50$, $n_i=0$, $\lambda=0.65\mu m$, $\mu=1$, $\mu_0=0.5$, $R=0.06$).

The atmospheric phase function p is

$$p=\frac{p_a\tau_a+p_R\tau_R}{\tau_0}\ , \tag{8}$$

where p_R is the molecular phase function, τ_R the molecular optical thickness, p_a the aerosol phase function, and τ_a the aerosol optical thickness.

(5) *Surface reflectivity*

The whitecap effect may be neglected, if the sea wind speed is smaller than 15 m / s.

For a dust storm case, the atmospheric condition may be treated as cloudy sky, and the reflectance of sea surface as Lambert surface characteristics. The relationship between wind speed and reflectivity is as follows (Payer 1982):

wind speed u (m / s)	sea surface albedo R
0	0.062
1.5	0.059
7.5	0.053
17.5	0.048

3. *Simulation calculation*

Carlson (1979) has derived the atmospheric aerosol thickness from satellite information of visible band (0.58–0.68μm) with accuracy as follows: While the aerosol thickness is smaller than 0.8, the error about 0.1–0.2; while the aerosol thickness is 0.8–2.0, the error about 0.2–0.4. Norton (1979) used the visible band information of GOES to derive aerosol thickness of Sahara dust on the Atlantic Ocean.

Kaufman (1982) take the Junge spectrum distribution with $v=3.0$, and $n_r=1.50$, $n_i=0$, $\lambda=0.65\mu$m, $\mu_0=\cos\theta_0=0.5$, $\mu=\cos\theta=1$. Surface reflectivity is Lambert diffusion. The relationship between reflective radiance I and atmospheric optical thickness τ_0 from Eq. (4) is shown in Fig. 6.

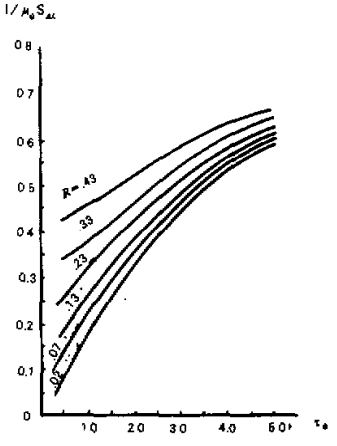

Fig. 6. Reflective radiance vs optical thickness with different surface reflectivities (Kaufman 1982).

I: reflective radiance of sunlight

$\pi S_{\Delta\lambda}$: solar constant

τ_0: optical thickness

R: reflectivity of surface

($v=3.0$. Junge distribution, $n_r=1.50$, $n_i=0$, $\lambda=0.65\mu m$, $\mu_0=\cos\theta_0=0.5$, θ_0= solar zenith angle, $\mu=\cos\theta=1$, θ: observation angle)

4. *Examples of EADS*

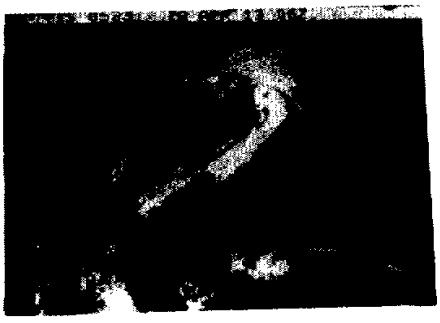

Fig. 7. GMS visible image of dust storm at 1400 BT 13 April 1979.

Fig. 8. GMS visible image of dust storm at 1400 BT 15 April 1979.

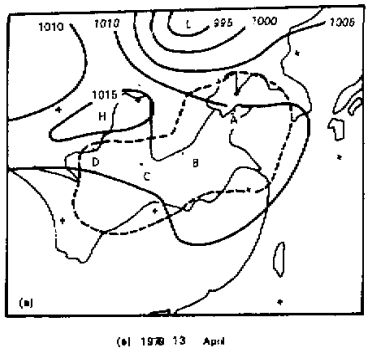

(a) 1979 13 April

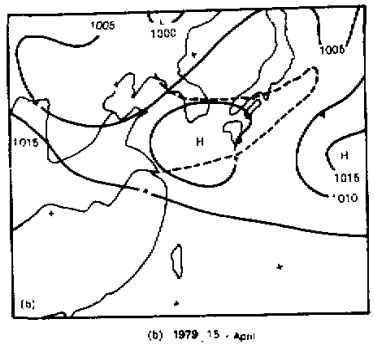

(b) 1979 15 April

Fig. 9. Surface pressure field (solid line) and area (dashed line) of the dust storm at 1400 BT, 13(a) and 15(b) April 1979.

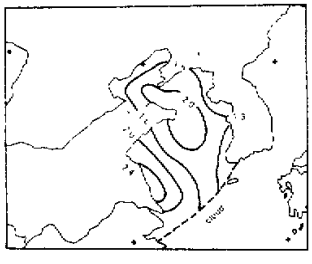

Fig. 10. Aerosol optical thickness distribution of the dust storm on 13 April 1979.

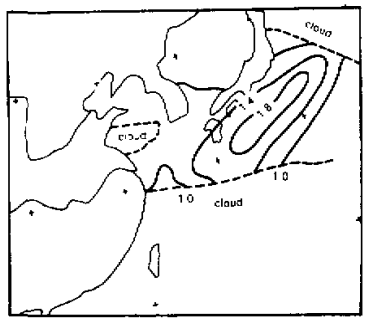

Fig. 11. Aerosol optical thickness of the dust storm on 15 April 1979.

The aerosol optical thickness can be derived from GMS VISSR (visible $\lambda=0.55$–$0.75\mu m$) observations. By formula (4), it is known that the atmospheric aerosol opti-

cal depth is a function of atmospheric reflectivity of sunlight $I^{\dagger} / S_{\lambda}\mu_0$. The refractivity is taken as $n_r = 1.50$ and $n_i = 0$, and the spectrum as Junge distribution with $v = 2.5$.

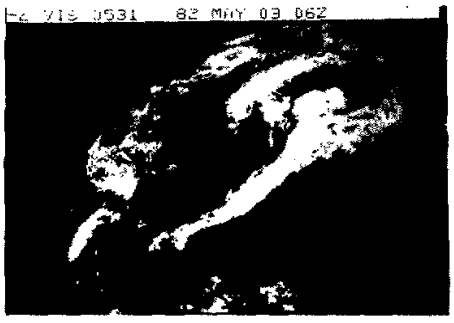

Fig. 12. GMS visible image of the dust storm at 1400 BT 3 May 1982.

Fig. 13. GMS visible image of the dust storm at 1400 BT 4 May 1982.

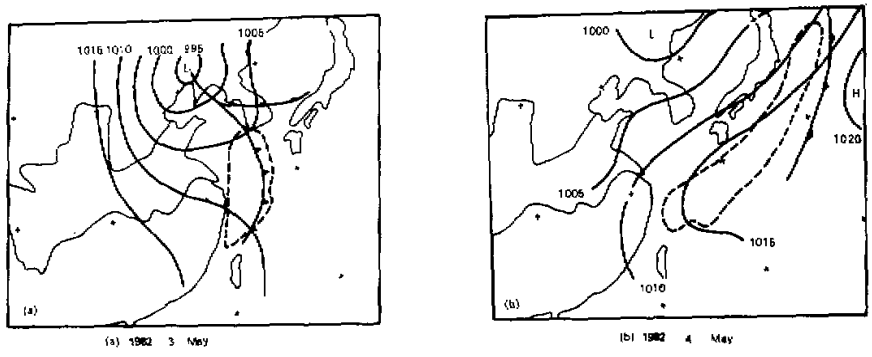

Fig. 14. Surface pressure field (solid line) and area (dashed line) of the dust storm at 1400 BT, 3(a) and 4(b) May 1982.

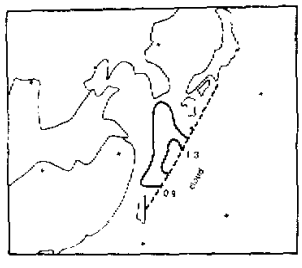

Fig. 15. Aerosol optical thickness distribution of the dust storm at 1400 BT 3 May 1982.

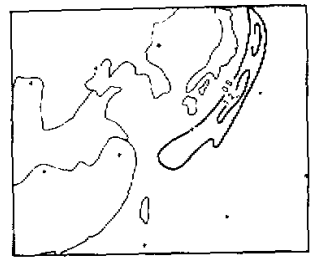

Fig. 16. Aerosol optical thickness distribution of the dust storm at 1400 BT 4 May 1982.

(1) The dust storm occurred in April 1979. The process of the Asian dust storm was associated with the activity of cold anticyclone. In the front of the anticyclone, the strong wind sent up the dust into the upper air. The dust storm could be found in GMS images, dated 13–15 April 1979. The GMS images and aerosol optical depth are shown in Figs. 7–11.

(2) The dust storm occurred in May 1982, which was caused by the southward displacement of the Mongolia cyclone. The strong wind sent up dust into the upper air. The GMS images and aerosol optical depth, dated 3–4 May 1982 are shown in Figs. 12–16.

III. SURFACE OBSERVATIONS

The atmospheric optical depth $\bar{\tau}$ could be derived from the ground–based actinometry by formula

$$S' = \left(\frac{D_0}{D}\right)^2 J_0 \cos\theta_0 e^{-m\bar{\tau}} , \tag{9}$$

where J_0 is the solar constant, D, D_0 the present and mean distance of sun–earth, θ_0 the solar zenith angle, m the atmospheric mass number, S' the solar radiation on the horizontal plane of meteorological station.

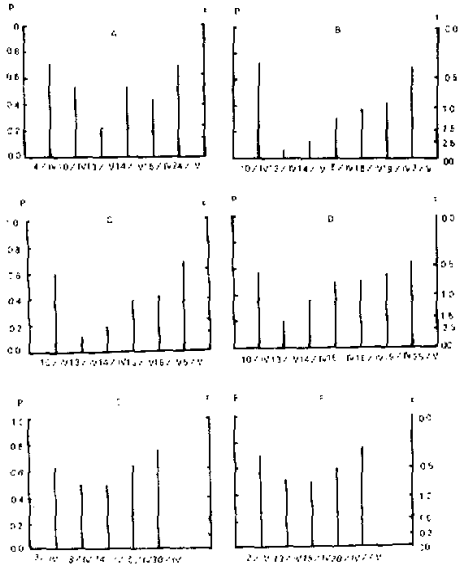

Fig. 17. Variation of atmospheric transmittance P. A: Yantai B: Zhengzhou C: Xi'an D: Lanzhou E: Yinchuan F: Taiyuan.

During the dust storm dated April 1979, according to the actinometry observations of A (Yantai), B (Zhengzhou), C (Xi'an) and D (Lanzhou), the optical depth of the dust storm could be derived. $\bar{\tau}$ and the atmospheric transmittance P are shown in Fig. 17.

To sum up these results, we got the distribution of atmospheric aerosol optical depth of the dust storm dated 13 April 1979, as shown in Fig. 18.

The variation of atmospheric optical thickness of dust storm measured with actinometry is listed in Table 1.

Although actinometry is the measurement of whole spectrum of solar radiation, the wavelength of mean aerosol attenuation falls in the range of 0.55–0.75μm ($\lambda = 0.63\mu$m). So that we can unite the results of satellite observation and those of ground–based actinometry

(Appendix I).

Fig. 18. Aerosol optical thickness of 13 April 1979 dust storm (satellite observation and surface actinometry).

Aerosol optical thickness on oceans and counter of dust storm are derived from satellite data; Aerosol optical thickness on land derived from surface actinometry.

A: Yantai, B: Zhengzhou, C: Xi'an, D: Lanzhou, E: Yinchuan, F: Taiyuan.

The lidar observations of the dust storm, dated 4 April 1979 in Nagoya, Nagoya University (Iwasaka, 1983) and 2 May 1979 in Beijing (Qiu, 1984) were carried out.

Table 1. The Variations of Atmospheric Optical Thickness τ and Aerosol Optical Thickness τ_a of Dust Storm

Station	Optical thickness of calm weather		Optical thickness of dust storm					
			13 April		14 April		15 April	
	τ	τ_a	τ	τ_a	τ	τ_a	τ	τ_a
A: Yantai	0.35	0.23	1.63	1.50	0.83	0.71	1.02	0.90
B: Zhengzhou	0.33	0.22	2.34	2.23	1.80	1.69	0.81	0.70
C: Xi'an	0.38	0.22	2.01	1.85	1.32	1.16	0.80	0.64
D: Lanzhou	0.44	0.24	1.50	1.30	1.01	0.81	0.72	0.52

IV. MASS LOAD

During the dust storm time, there exists the relationship between the aerosol optical depth τ_a and its mass load M_v.

$$M_v = k\tau_a , \quad (g/m^2) \tag{10}$$

where k is a constant. Some scientists pointed out that $k = 3.75 \times 10^6$ at the source of Sahara dust storm, and $k = 4.2 \times 10^5$ after the long transport of the dust storm till the Caribbean Sea.

Let $k = 1.63 \times 10^6$ in Asian dust storm (Appendix II).

Two examples of Asian dust storm, dated April 1979 and May 1982 have been discussed. The aerosol optical thickness is derived from GMS satellite observation and actinometry of surface observation. Thus the mass load of these dust storms is approximately $1-8 \times 10^6$ ton.

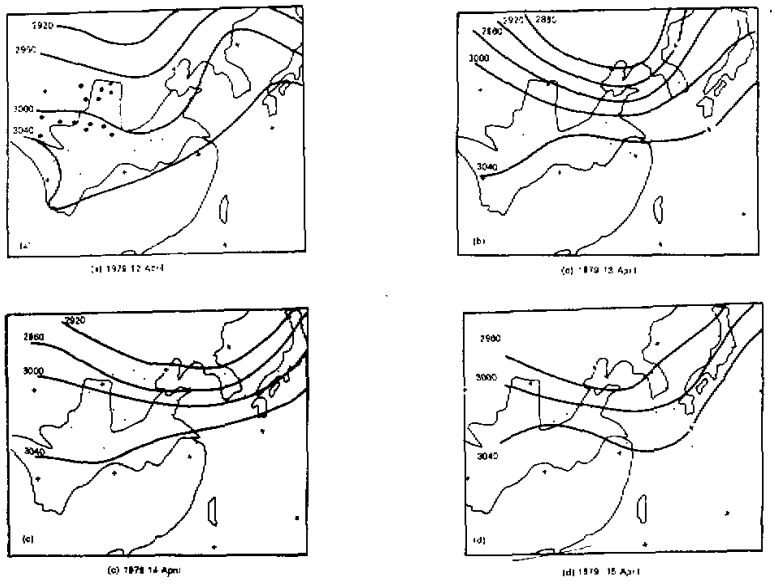

Fig. 19. 700 hPa stream field and surface data of sand storm and floating dust for 12 (a), 13(b), 14(c), and 15(d) April 1979. ○ sand dust, floating dust, ⊗ sand dust and floating dust.

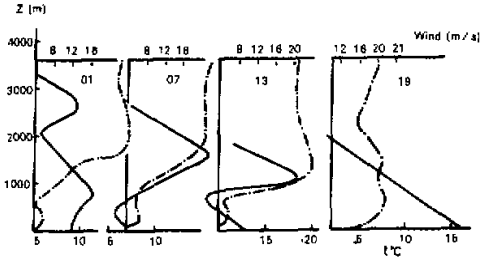

Fig. 20. Variations of temperature and wind profiles of dust storm, Beijing 18 April 1980 (Zhou, 1981).

V. WEATHER ANALYSIS OF DUST STORM

The surface pressure field, surface data of sand dust and floating dust, and 700 hPa stream line are shown in Fig. 19.

In April 18–20, 1980, there was a dust storm weather, accompanied with cold wave, coming from Siberia.

The variation of meteorological elements is shown in Fig. 20. There existed a strong temperature inversion and wind shear. The concentration of dust was 4×10^{5}–2.5×10^{-4}g/m^3, with a maximum of 6.13×10^{-3}g/m^3. As to the size of particulate, on reference days, the diameter of maximal density was 0.4μm; on dust storm days it was 0.6–1μm. The particulate of dust storm is larger than that of common aerosol. In order to analyse the composition of particulate, the concentration of elements in the aerosol might be detected by chemical method (fluorescence analysis). The results (Zhou, 1981) have shown that there exists a large dif-

ference of aerosol composition between samples on reference and storm days. It suggests that the dust storm source may not only come from loess area. From the potential temperature analysis and lidar observation, Iwasaka (1983) suggested that the trajectory of dust storm may have two ways, one comes from Mid-Asia, the other comes from Mogolia.

VI. THE AEROSOL CONTENT OVER SEA SURFACE

1. *Treatment of Sea Surface Reflectivity*

In the clear sky, the sea surface reflectivity may be treated as a bidirectional reflection process.

If the atmospheric effect on sea surface reflection is neglected, the sunlight (intensity $I_0=\pi S_\lambda$) would be reflected in all directions by wave facets of sea surface. Let $I(\theta_0, \theta, \varphi)$ be the reflected radiance in direction (θ, φ).

By the definition of $\eta(\theta_0, \theta, \varphi)$, we have

$$\eta(\theta_0, \theta, \varphi)=\frac{\pi I(\theta_0, \theta, \varphi)}{F(\theta_0)} , \tag{11}$$

where $F(\theta_0)$ is the total reflective flux of sea surface, i.e.

$$F(\theta_0)=\iint_{\text{hemisphere}} I(\theta_0, \theta, \varphi)\cos\theta\sin\theta d\theta d\varphi. \tag{12}$$

The flux intensity $R(\theta_0)$ is then

$$R(\theta_0)=\frac{F(\theta_0)}{\pi S_\lambda \cos\theta_0} . \tag{13}$$

The reflectivity $\gamma(\theta_0, \theta, \varphi)$ in the (θ, φ) direction is written as

$$\gamma(\theta_0, \theta, \varphi)=\frac{I(\theta_0, \theta, \varphi)}{\pi S_\lambda \cos\theta_0} . \tag{14}$$

The parameters γ, R and $\eta(=\frac{\pi\gamma}{R})$ have been derived with the statistical theory of sea wave.

The inclination probability of wave facets of sea surface may be expressed as a Gaussian distribution, i.e.,

$$p(z_x, z_y)=\frac{1}{\pi\sigma^2}\exp\left[-\frac{z_x^2+z_y^2}{\sigma^2}\right], \tag{15}$$

where z_x, z_y are the inclination of tangent plane along x and y axes respectively. x axis is found in the solar plane. $p(z_x, z_y)$ is the probability density of the inclination, σ is the RMS deviation of inclination, depending on the sea breeze, i.e.,

$$\sigma^2=0.003+0.00512u\pm 0.004, \tag{16}$$

where u is the wind speed in m / s.

The reflected radiance $Id\Omega$ is contributed by a certain facet with the inclination within the range $z_x \to z_x+dz_x$, $z_y \to z_y+dz_y$. The facet reflection can be treated as a mirror reflection. So that

$$I(\theta_0, \theta, \varphi)d\Omega=\pi S_\lambda \cos\theta_0 \rho(\omega)p(z_x, z_y)dz_x dz_y, \tag{17}$$

where ω is the angle between the incident ray and normal of facet, $\rho(\omega)$, the mirror

reflectivity; $(\theta_0, 0)$, the incident angle; and (θ, φ), the observing angle (Fig. 21).

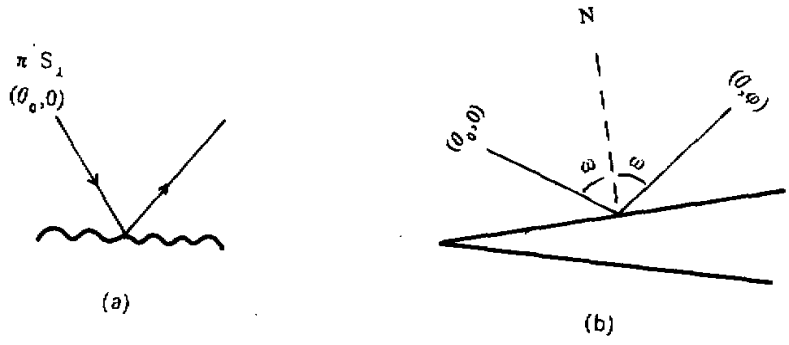

Fig. 21. Sunlight reflectance from rough sea surface.

From the geometric analysis, $p(z_x, z_y)dz_x dz_y$ can be expressed as

$$p(z_x, z_y)dz_x dz_y = \frac{a}{\pi\sigma^2(\cos\theta + \cos\theta_0)}\exp\left[\frac{1-2a}{\sigma^2}\right]d\Omega, \tag{18}$$

$$a = \frac{1 + \cos\theta\cos\theta_0 + \sin\theta\sin\theta_0\cos\varphi}{(\cos\theta + \cos\theta_0)^2}, \tag{19}$$

and

$$\cos^2\omega = \frac{1}{2}(1 + \cos\theta\cos\theta_0 + \sin\theta\sin\theta_0\cos\varphi). \tag{20}$$

By formulas (14), (17) and (18), we have

$$\gamma(\theta_0, \theta, \varphi) = \rho(\omega)\frac{a}{\pi\sigma^2(\cos\theta + \cos\theta_0)}\exp\left[\frac{(1-2a)}{\sigma^2}\right], \tag{21}$$

where

$$\rho(\omega) = \frac{1}{2}(\rho_H + \rho_V);$$

$$\rho_H(\omega) = \left|\frac{n^2\cos\omega - \sqrt{n^2 - \sin^2\omega}}{n^2\cos\omega + \sqrt{n^2 - \sin^3\omega}}\right|^2;$$

$$\rho_V(\omega) = \left|\frac{\cos\omega - \sqrt{n^2 - \sin^2\omega}}{\cos\omega + \sqrt{n^2 - \sin^2\omega}}\right|^2;$$

in which n is the refractivity of sea water, while the reflectivity is

$$R = \int_0^{2\pi}\int_0^{\pi/2}\gamma(\theta_0, \theta, \varphi)\cos\theta\sin\theta d\theta d\varphi. \tag{22}$$

2. *The Aerosol Content over Sea Surface*

In clear sky, the aerosol content can be measured by satellite AVHRR visible image of NOAA-7. The AVHRR visible channel is between 0.58–0.68μm. The color images are supplied by the Satellite Meteorology Center of China. The value of $I/\pi S_\lambda\cos\theta$ can be ob-

tained from the iso–reflectivity diagram (πS_λ is the solar constant of waveband 0.58–0.68μm). The relationship between the aerosol optical thickness and the reflected radiance of sunlight may be established by the radiative transfer equation (4). Figs. 22 and 23 are surface pressure field and the regional brightness image of Bohai Bay at 15:07 BT (Beijing Time) 28 November 1984. Fig. 24 is the iso–reflectivity diagram.

Because of the river sand, the reflectivity near the coast reveals non–uniform characteristics. Then the reflectivity of the east part of Bohai Bay is taken to measure the atmospheric aerosol optical thickness. The parameters in Eq. (4) are assumed as follows: the particulate spectrum is taken as the Junge distribution with $v=3.3$ and the refractivities are $n_r=1.50$ and $n_i=0.01$, the refractivity of sea water is $n=1.33$, the wind speed above oceans is 6 m / s, the solar zenith angle θ_0 is 43°, the nadir angle of observation $\theta=27°$, and azimuth angle $\varphi=40°$.

From formulas (21) and (22), we have got the reflectivity on the Bohai Bay R = 2.5% and obtained:

the spectrum region	0.58–0.68μm
the aerosol optical thickness	0.192

The results are in agreement with those of Takashima (1981).

VII. CONCLUSION

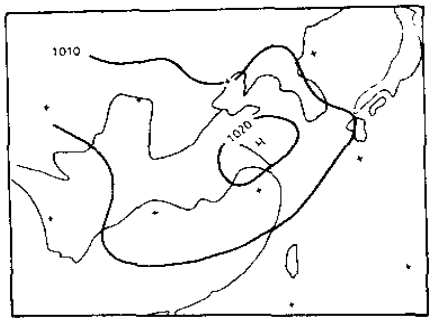

Fig. 22. Surface pressure field of calm weather, 28 November 1984.

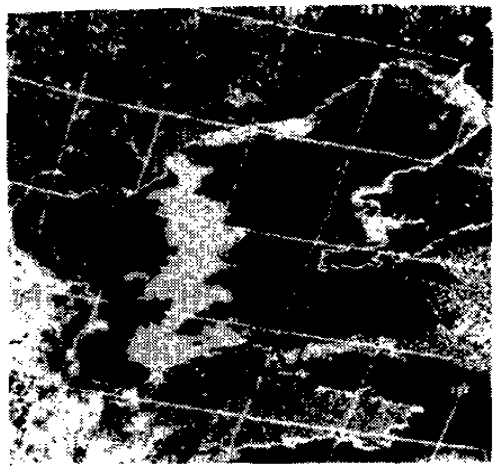

Fig. 23. The brightness image of AVHRR (visible) of NOAA–7 on 28 November 1984.

Fig. 24. Iso–reflectivity diagram of NOAA–7 AVHRR (visible) of Bohai Bay on 28 November 1984. ($R=2.5\%$, $\tau_a=0.192$).

The increase in atmospheric aerosol affects global climate and human life. The EADS is an important source of atmospheric aerosol.

The satellite observations can be used to detect the aerosol optical thickness on oceanic surface. Combining them with ground-based instruments (actinometer, lidar etc.) is able to obtain the distribution of aerosol optical thickness for dust storms.

REFERENCES

Carlson T.K. (1979), *Monthly Weather Review*, **107**: 322–335.
Griggs M., Satellite measurements of atmospheric aerosol, AD–AO66744.
Iwasaka Y., H. Minoura, K. Nogaya (1983), *Tellus*, **35B**: 959–970.
Kaufman Y.J., J. H. Joseph (1979), *Journal of Geophysical Research*, **84C**: 3165–3172.
Kaufman Y.J., J. H. Joseph (1982), *Journal of Geophysical Research*, **87C**: 1287–1299.
Norton C. C., F.R. Mosher, B. Hinton, D.W. Martin, D. Santek, W. Kakklow (1980), *Journal of Applied Meteorology*, **19**: 959–970.
Otterman J.R., R.S. Fraser, O.P. Baheti (1982), *Journal of Geophysical Research*, **87C**: 1270–1278.
Parrigton J.R., W.H. Zoller, N.K. Aras (1983), *Sciences*, **220**: 195–197.
Payer R.E. (1982), *Journal of Atmospheric Science*, **24**: 959–970.
Qiu Jinhuan, Zhao Yanzeng, Wang Hongqi (1984), *Scientia Atmospherica Sinica*, **8**: 205–210.
Saunder P.M. (1967), *Journal of Geophysical Research*, **72**: 4643–4649.
Takashima T., T. Takayama (1981), *Papers in Meteorology and Geophysics*, **32**: 267–274.
Zhang Deer (1984), *Scientia Sinica*, **27B**: 825–886.
Zhou Mingyu (1981), *Kexue Tongbao*, **26**: 609–611.

Appendix I. Optical Thickness Measured with Actinometry and the Characteristics of Optical Thickness Spectrum.

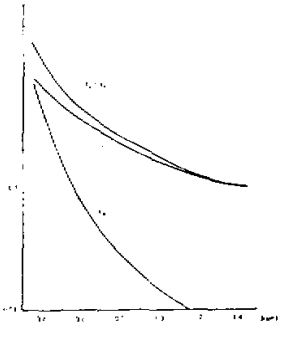

Fig. 1*. τ_a and τ_R spectra.

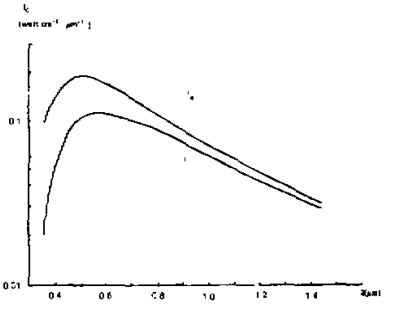

Fig. 2*. I_0 and I spectra.

By Angstrom's formula, aerosol optical thickness τ_a can be written as

$$\tau_a = \beta' \lambda^{-\alpha'} . \tag{1}$$

In Beijing, $\alpha' = 1.45$ and averaged maximum aerosol optical thickness at 0.5μm wavelength $\tau_{a0.5} = 0.44$. (Zhao 1984, 1988). Therefore, the aerosol optical thickness spectrum

$$\tau_a = \tau_{a0.5} \left(\frac{0.5}{\lambda} \right)^{1.45} . \tag{2}$$

The molecular optical thickness

$$\tau_R = C\lambda^{-4}, \tag{3}$$

where C is constant. In Beijing, averaged molecular optical thickness at 0.5μm wavelength $\tau_{R0.5} = 0.151$. Its spectrum

$$\tau_R = \tau_{R0.05}\left(\frac{0.5}{\lambda}\right)^4 . \tag{4}$$

τ_a and τ_R spectra are shown in Fig.1*. When one atmosphere thickness is taken, then

$$I = I_0 \exp -(\tau_a + \tau_R), \tag{5}$$

where I is the solar radiation on the ground surface, I_0 solar radiation at the top of atmosphere, taken from Paltridge and Platt (1976). I_0 and I, derived from formula (5), are shown in Fig. 2*. By formula (5), the optical thickness in 0.35μm–1.4μm waveband is 0.37, which is equal to optical thickness of $\lambda_m = 0.63\mu$m.

The wavelength of GMS satellite remote sensing is between 0.55μm–0.75μm. From Fig. 1*, the averaged optical thickness is 0.37 also. It corresponds to the results at averaged wavelength $\lambda_m = 0.63\mu$m.

Appendix II. Columnar Aerosol Mass M_V and Aerosol Optical Thickness.

Junge aerosol spectrum

$$n(r) = \frac{dN}{dr} = Cr^{-(v+1)}. \tag{1}$$

Columnar aerosol mass M_V is

$$M_V = \int_0^\infty \rho_v dZ, \tag{2}$$

where ρ_v aerosol mass of unit volumn air,

$$\rho_v = \int_{r_1}^{r_2} \rho \frac{4}{3}\pi r^3 n(r)dr = \rho \frac{4}{3}\pi c\left(\frac{2\pi}{\lambda}\right)^{v-3} \int_{\alpha_1}^{\alpha_2} \alpha^{-(v-2)} d\alpha , \tag{3}$$

ρ density of aerosol particulate, $\alpha = \frac{2\pi r}{\lambda}$.

τ_a Aerosol optical thickness:

$$\tau_a = \int_0^\infty \beta_{sc} dZ \tag{4}$$

β_{sc} scattering coefficient:

$$\beta_{sc} = c\pi\left(\frac{2\pi}{\lambda}\right)^{v-2} \int_{\alpha_1}^{\alpha_2} \frac{Q_{sc}}{\alpha^{v-1}} d\alpha , \tag{5}$$

Q_{sc} relative cross section of Mie scattering.

From formulas (1)–(5), we have

$$\frac{M_v}{\tau_a} = \frac{4}{3}\rho\frac{\lambda}{2\pi} \frac{\int_{\alpha_1}^{\alpha_2} \alpha^{-(v-2)} d\alpha}{\int_{\alpha_1}^{\alpha_2} Q_{sc}\alpha^{-(v-1)} d\alpha} . \tag{6}$$

Let $v = 2.5$, $\lambda = 0.65\ \mu$m, $r_1 = 0.1\ \mu$m, $r_2 = 15\ \mu$m, $\rho = 2.5\ \mathrm{g/cm^3}$, then

$$M_v = 1.63\tau_a\ \mathrm{g/m^2} . \quad (\mathrm{ton/km^2}) \tag{7}$$

Paltridge G.W. and C.M.R. Platt (1976), *Radiative Processes in Meteorology and Climatology*, Elservier, New York.

Zhao Bolin et al. (1984), *Scientia Sinica*, **27**(B): 407–419.

Zhao Bolin et al. (1988), *Aerosol and Climate*, Edited by P. V. Hobbs and M.P. McCormick, A. Deepak Publishing Hampton, 89–100.